International Journal of Concrete Structures and Materials

RESEARCH

Open Access

Multi-objective Optimization of Mix Proportion for Volcanic Scoria Concrete Using Response Surface Methodology

Bin Cai[1], Li Xu[1], Lin Wang[2] and Feng Fu[3*]

Abstract

Due to the scarcity of natural sand resources and the abundance of volcanic scoria sand, volcanic scoria sand concrete is becoming increasingly popular. Therefore, this paper aims to study the mix proportion of new sustainable steel fiber reinforced volcanic scoria sand concrete (SFVSSC). Response surface methodology (RSM) was used to design the mix proportion according to the recommendations of EFNARC 2005 using the proportion of water-to-cement ratio (w/c) (0.35, 0.4, and 0.45), the volcanic scoria sand replacement rate (Rvs) (25, 50, and 75%), and steel fiber volume content (Vsf) (0.5, 1, and 1.5%) as input variables. To assess the workability and mechanical properties of SFVSSC using RSM, slump, thermal conductivity, specific strength, compressive strength, and splitting tensile strength were determined. The results show that the quadratic polynomial regression equation can be used to predict the effect of different composition factors on the performance of SFVSSC with high accuracy and confidence. In addition, stress–strain curves were obtained for mixtures with different Rvs and Vsf. Finally, multi-objective optimization produced optimal mix proportions for SFVSSC: w/c of 0.35, Rvs of 52.8%, and Vsf of 1.15%. The optimization results were verified experimentally, and the absolute value of the relative error between the predicted and tested strength values was less than 5%. This paper shows that it is feasible to use SFVSSC and suggests the potential application of RSM in concrete proportioning.

Keywords Volcanic scoria, Steel fiber, Mix proportion, Response surface methodology, Multi-objective optimization

1 Introduction

Concrete is the world's most widely used construction material and the second most commonly used material (Li et al., 2023). Globally, more than 10 billion cubic meters of concrete are produced yearly, making it one of the world's largest consumers of natural resources (Miller et al., 2016). Sand is one of the necessary ingredients for concrete, and its dosage is about 30% of the total weight of concrete (Luo et al., 2023). In recent years, with increased infrastructure construction in developing countries and infrastructure renovation in developed countries, concrete consumption by the construction industry has increased, and global demand for sand exceeds 8 billion tons per year, leading to the rapid depletion of natural sand (Yifru et al., 2020). From the perspective of environmental protection and sustainable development, natural sand can no longer meet the current construction demand. Therefore, looking for substitutes such as industrial waste, etc., is necessary (Tunc, 2019).

In contrast, manufactured sand uses a wide range of materials, such as industrial slag, mine tailings, concrete

Journal information: ISSN 1976-0485/eISSN 2234-1315.

*Correspondence:
Feng Fu
feng.fu.1@city.ac.uk
[1] School of Civil Engineering, Jilin Jianzhu University, Changchun, China
[2] School of Economics and Management, Jilin Jianzhu University, Changchun, China
[3] Department of Engineering, School of Science and Technology, City, University of London, London, UK

waste, recycled aggregates, and other solid waste that can be used as raw materials for production. In northeast China, there are abundant resources of volcanic scoria, and fine-grained sand from volcanic scoria deposits is underutilized as a construction material (Tchamdjou et al., 2017a, 2017b). Volcanic scoria, as a new type of environmentally friendly building material with a vast source and low cost, has low density, porous structure, lightweight, high fire resistance, low modulus of elasticity, good water absorption properties, high frost and corrosion resistance and durability, good thermal insulation, etc., and can be used as both structural and non-structural concrete use (Huang et al., 2023). Volcanic scoria reserves in the area, with the preparation of lightweight aggregate concrete (LWAC) for the actual project, can save a lot of energy for the country, meet the energy efficiency requirements in buildings, and reduce the structure's weight, achieving the goal of green environmental protection. In recent decades, many researchers have studied the feasibility of volcanic scoria as a fine aggregate for concrete. In many countries around the world, volcanic scoria has been used as an aggregate for producing lightweight mortar or concrete (Anwar Hossain, 2004; Tchamdjou et al., 2017a, 2017b). Tchamdjou et al., (2017a, 2017b) concluded that using volcanic scoria as sand (volcanic scoria sand) in the manufacture of silicate cement mortar increased the mechanical strength of the mortar. Tchamdjou et al., (2017a, 2017b) also conducted a study using volcanic scoria from ' Djoungo ' (Cameroon) as cement and fine aggregate to replace Portland cement mortar. They concluded that the volcanic scoria sand reduced the self-weight of the mortar and showed that the mechanical strength decreases during the early curing period (up to 90 days) compared to conventional mortar. Still, the obtained mortar can be used for further applications in masonry, confirming that volcanic scoria can be used as a resource for producing cement, mortar, and concrete. Compared to normal concrete, volcanic scoria fine aggregate concrete is lighter in unit weight and, therefore, has weaker mechanical properties and more brittle material. These drawbacks hinder its wide application in civil engineering (Li et al., 2019; Zhou et al., 2016).

An effective way to solve these problems is to add fiber as an additional raw material (Li et al., 2019). In some work, metallic fibers (e.g., steel fibers) have improved the flexural strength and splitting tensile strength of LWAC (Liu et al., 2019). Basser et al. (2022) showed that steel fibers transfer stresses through both sides of the bridging crack, thereby increasing concrete's tensile strength, flexural strength, and energy absorption capacity. Afroughsabet et al. (2015) showed that increasing the steel fiber volume content improves the mechanical properties of concrete. This is due to the ability of fibers to prevent crack extension, reduce stress concentration at the crack tip and retard crack expansion. Hassanpour et al. (2012) reported that compressive strength and strain corresponding to peak stress increased with the addition of steel fibers. The maximum compressive strain of concrete with steel fibers was higher than that of plain concrete. The appropriate steel fiber volume can increase the compressive strength of LWAC. However, when steel fiber volume content exceeds a specific range, its mechanism of action is undermined (Liu et al., 2019). Therefore, this paper adds steel fibers (SF) to improve the properties of volcanic scoria sand concrete.

To expand the application of SFVSSC, it is necessary to carry out a comprehensive and systematic study of its performance characteristics; the performance characteristics, mechanical properties, and durability in terms of mix proportion, which is a prerequisite for the study of its performance characteristics (Huang et al., 2022). RSM has recently gained popularity in civil engineering to simulate or forecast performance and eventually accomplish multi-objective optimization (Luo et al., 2023). According to Zhang et al.'s (2018) mechanical property and durability tests on mortar containing pozzolanic cementitious material, RSM is an effective technique for optimizing mortar design parameters. Adamu et al., (2018, 2021) investigated the effect of fly ash and plastic waste on the mechanical properties of concrete, and the results of RSM-based tests were satisfactory. Asadzadeh et al. (2018) emphasized that the model created from RSM enables the prediction of values for density, compressive strength, and cost response, all of which are relevant for various foamed concrete applications. Safari et al. (2018) obtained mix parameters for self-compacting concrete with optimal mechanical and workability by RSM, including rice husk ash and macro-synthetic fibers. Therefore, we have recognized the feasibility of using RSM to evaluate and optimize the mechanical properties of concrete. On the other hand, volcanic scoria sand in northern China is widely spread and is an abundant resource that can be utilized economically and environmentally friendly. In summary, it is essential for multi-objective optimization of the mix proportion for SFVSSC using RSM.

This study aims to provide a method to optimize the mix proportion of volcanic scoria sand (VS) in concrete and promote using VS in concrete. Volcanic scoria is used as fine aggregate to replace some natural sand (NS). Seventeen concrete formulations were developed using the Box-Benken method (BBD), considering w/c, Rvs, and Vsf as influencing factors. Then, the effects of the above factors on slump, thermal conductivity, specific strength, compressive strength, and splitting tensile strength were investigated

using RSM. The stress–strain curve of SFVSSC was established. Finally, the mix proportion of SFVSSC was optimized for SFVSSC, and the optimized mix proportion was verified. The optimal SFVSSC shows suitability and mechanical properties to be used for overall green building design, which is in line with the strategy of green concrete production (Luo et al., 2023; Warati et al., 2019).

2 Response Surface Methodology (RSM)

The RSM combines statistics and mathematics to create an experimental model. It also comprises fitting the regression surface to get a close-range response (Abdulkadir et al., 2022). It's a sophisticated statistical technique frequently applied to process and experiment simulation (Siamardi, 2022). In this procedure, the essential variables are first identified, and then the impacts of the variables are modeled and examined using mathematical and statistical tools. The variables under study and the test results are given mathematically (Amiri et al., 2022; Basser et al., 2022). This technique displays the impact of two input factors on the response in contour and three-dimensional formats (Shahrul et al., 2021). These formats help predict the output produced over the range of variable changes. Compared to orthogonal tests, RSM has the advantage of high precision, fewer experiments, the ability to study interactions between multiple factors, and the ability to predict target values obtained from different levels of factors, which are widely used in process optimization and improving product parameters (Luo et al., 2023).

RSM can be divided into full factorial experimental design, central composite design (CCD), Box-Behnken experimental design, and so on. The Box-Behnken Design is independent quadratic design that is rotatable and requires three factorial levels; the Box–Behnken design considers the effects of different factors sequentially, holding all other factors constant when considering the impact of a single factor (Hari et al., 2023). Therefore, BBD is used as the experimental design method in this paper.

The response values are optimized, the quadratic prediction model (Eq. 1) for ideal response conditions is identified, the process parameters are optimized, and the multivariate optimization is successfully solved using the BBD model and analysis of multiple variables affecting the response values (Yifru et al., 2020).

$$y = \beta_0 + \sum_{1}^{k} \beta_i x_i + \sum_{1}^{k} \beta_{ii} x_i^2 + \sum \sum_{i<j} \beta_{ij} x_i x_j + \varepsilon \quad (1)$$

where y is the response variable, x_i and x_j are the process variables, k is the number of process variables, β is the intercept, and ε is the random error.

3 Materials Preparation

3.1 Materials

The design tests were carried out using SFVSSC according to the Chinese Standard (JGJ/T12-2019, 2019). The cement used was ordinary silicate cement P.O 42.5 with a density of 3.1 g/cm^3. It uses both NS and VS types of fine aggregates. The former has a fineness modulus of 2.1, and the latter is prepared from Huinan County, Jilin Province, China, with a fineness modulus of 2.5. The chemical composition of the VS is listed in Table 1. The coarse aggregate was made up of crushed stone with a maximum particle size of 12.5 mm. The materials used are shown in Fig. 1. The properties of the steel fibers are shown in Table 2. The physical properties of the two sands and the gradation curves are shown in Table 3 and Fig. 2, respectively.

3.2 Mix Proportions

The three variables used in this study—w/c, Rvs, and Vsf—were altered as independent variables at three different levels (Maaze et al., 2023), according to Table 4. The studied mixing plan was based on the test locations in Fig. 3, as shown in Table 5.

Using the BBD method, the number of the investigated tests (N) was calculated as follows:

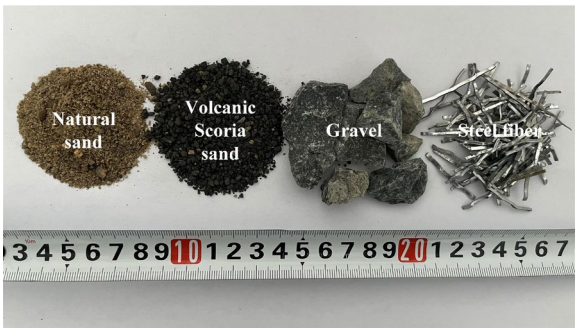

Fig. 1 Materials

Table 1 Chemical composition of volcanic scoria sand (%)

SiO_2	Al_2O_3	TFe_2O_3	CaO	MgO	K_2O	Na_2O	TiO_2	P_2O_5	LOI	MnO
67.85	14.50	3.55	2.24	0.85	2.59	2.56	0.51	0.10	5.04	0.09

Table 2 Physical properties of steel fibers

Material	Length (mm)	Width (mm)	Thickness (mm)	Equivalent diameter (mm)	Aspect ratio	Density (g/cm^3)
Steel fiber	38	1	0.35–0.5	0.76	50	7.8

Table 3 Physical properties of sand

Materials	Bulk density (kg/m^s)	Apparent density (kg/m^3)	Porosity (%)	Clay content (%)
Natural sand	1424	2610	45.4	0.7
Volcanic scoria sand	1178	2360	50.0	1.1

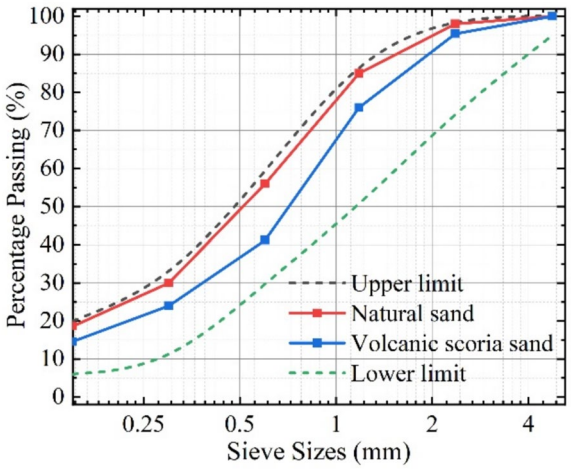

Fig. 2 Particle size distribution (PSD) diagram of aggregates

Table 4 Factors and level of the test

Variable	Symbol	Levels		
		− 1	0	1
w/c	A	0.35	0.4	0.45
Rsv (%)	B	25	50	75
Vsf (%)	C	0.5	1	1.5

$$N = 2k(k-1) + C_p \tag{2}$$

where k is the number of factors. In this study, $k=3$, and C_p is the number of center points, considering $C_p=5$. Experimenting again at the center point lessens the impact of random mistakes on the model, resulting in acceptable accuracy. The main stages of this study are briefly depicted in Fig. 4.

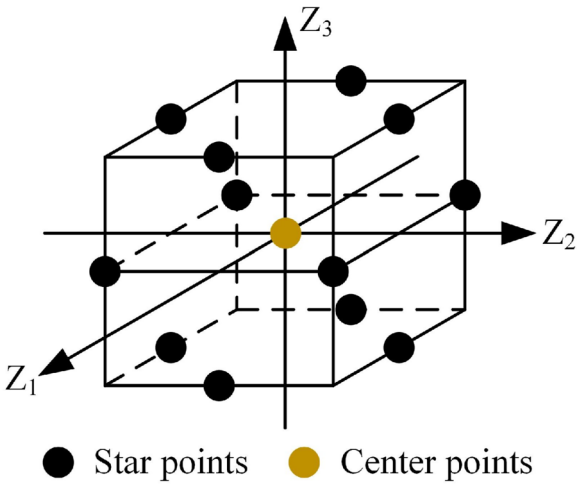

Fig. 3 Designed matrix for k = 3 using BBD

3.3 Mix Preparation

The Chinese Standard (GB/T 50081-2019, 2019) was used to conduct the mechanical test. First, the concrete mixer was subjected to slurry treatment. Next, the weighted cement, NS, VS, gravel, and SF were added to the mixer. The mixture was then left drying for 30 s, and water was then added and stirred for 120 s. The SFVSSC was thoroughly mixed, poured into a test mold previously coated with a release agent, and then placed on a vibrating table for vibration. Excessive vibration must be avoided to prevent the concrete from segregating and reducing the bond strength between the fibers and the substrate. The specimen was then flattened with a spatula, and the test mold was labeled. After 24 h, the mold was taken out. The preparation process is shown in Fig. 5. Finally, the specimens spent 28 days in the curing pool.

3.4 Testing Methods

With the increasing development of modern engineering structures in the direction of large spans, heavy loads, and tall towers, structures face the problem of reducing cross-sectional area, reducing structural self-weight, and improving thermal insulation in many ways. Most of the research on LWAC has focused on obtaining high-strength structural load-bearing or non-structural materials with low thermal conductivity. Few studies have focused on balancing mechanical and thermal properties.

Table 5 Mix proportions of concrete (unit: kg/m^3)

No.	w/c	Rvs	Vsf	C	NS	VS	G	SF	WA	W	FA	SiF
1	0.35	25	1	462.2	586.7	159.1	1155.6	62.3	4.27	166	81.3	20.6
2	0.45	25	1	353.2	586.7	159.1	1155.6	62.3	4.27	166	81.3	20.6
3	0.35	75	1	462.2	195.6	476.9	1155.6	62.3	4.27	166	81.3	20.6
4	0.45	75	1	353.2	195.6	476.9	1155.6	62.3	4.27	166	81.3	20.6
5	0.35	50	0.5	462.2	391.1	317.9	1155.6	31.3	4.27	166	81.3	20.6
6	0.45	50	0.5	353.2	391.1	317.9	1155.6	31.3	4.27	166	81.3	20.6
7	0.35	50	1.5	462.2	391.1	317.9	1155.6	93.6	4.27	166	81.3	20.6
8	0.45	50	1.5	353.2	391.1	317.9	1155.6	93.6	4.27	166	81.3	20.6
9	0.4	25	0.5	403	586.7	159.1	1155.6	31.3	4.27	166	81.3	20.6
10	0.4	75	0.5	403	195.6	476.9	1155.6	31.3	4.27	166	81.3	20.6
11	0.4	25	1.5	403	586.7	159.1	1155.6	93.6	4.27	166	81.3	20.6
12	0.4	75	1.5	403	195.6	476.9	1155.6	93.6	4.27	166	81.3	20.6
13	0.4	50	1	403	391.1	317.9	1155.6	62.3	4.27	166	81.3	20.6
14	0.4	50	1	403	391.1	317.9	1155.6	62.3	4.27	166	81.3	20.6
15	0.4	50	1	403	391.1	317.9	1155.6	62.3	4.27	166	81.3	20.6
16	0.4	50	1	403	391.1	317.9	1155.6	62.3	4.27	166	81.3	20.6
17	0.4	50	1	403	391.1	317.9	1155.6	62.3	4.27	166	81.3	20.6

Cement, NS: Natural sand, VS: Volcanic scoria sand, G: Gravel, SF: Steel fiber, WA: Water-reducing agent, W: Water, FA: Flyash, SiF: Silica Fume

For this reason, SFVSSC has been studied regarding slump, thermal conductivity, specific strength, compressive strength, splitting tensile strength, and stress–strain tests (Huang et al., 2013; Sayadi et al., 2016; Wu et al., 2015; Yu et al., 2015).

3.4.1 Workability

The slump test was used to determine the workability of fresh concrete mixtures according to the Chinese Standard (GB/T50080-2016, 2016). Fig. 6 shows the slump test diagram.

3.4.2 Thermal Conductivity

The thermal conductivity of concrete was tested according to the Chinese Standard (GB 10294-2008, 2008), and 300 mm × 300 mm × 30 mm concrete specimens are made. A fully automatic thermal conductivity tester was used to determine the thermal conductivity of concrete. According to the one-dimensional steady-state heat transfer equation, the heat generated by the hot plate heater was transferred to the cold plate through the test specimen and outside the system through the circulating water in the cold plate and other work to form a thermal cycle. The test setup is shown in Fig. 7. The equation for thermal conductivity was as follows:

$$\lambda = \frac{\boldsymbol{\Phi} d}{A(T_1 - T_2)} \tag{3}$$

where λ is the coefficient of thermal conductivity, Φ is the average heating power of the measuring section of the heating unit, d is the average thickness of the specimen, T_1 is the average temperature of the hot surface of the specimen, T_2 is the average temperature of the cold surface of the specimen, and A is the measuring area.

3.4.3 Specific Strength

Specific strength, which can be used as an index to gauge a material's lightweight and high strength, is described as the ratio of the 28-day compressive strength to the dry apparent density (Li et al., 2021). According to the Chinese Standard (GB/T50080-2016, 2016), concrete specimens measuring 100 mm × 100 mm × 100 mm were created. The dry density was determined for each group of specimens by standard curing to 28 days and then drying in a drying oven. The specific strength was calculated from Eq. 4:

$$f_s = \frac{f_c}{\boldsymbol{\rho}_d} \tag{4}$$

where f_s is the specific strength of the concrete cube specimen, f_c is the compressive strength of the concrete cube specimen, and ρ_d is the dry density of the concrete specimen.

3.4.4 Mechanical Properties Testing

The compressive and splitting tensile strength were tested on 100 mm cubic specimens in accordance with the Chinese Standard GB/T 50081-2019. Three replicates were used for each test group. The tests were conducted using a YAW-1000 testing machine with loading rates

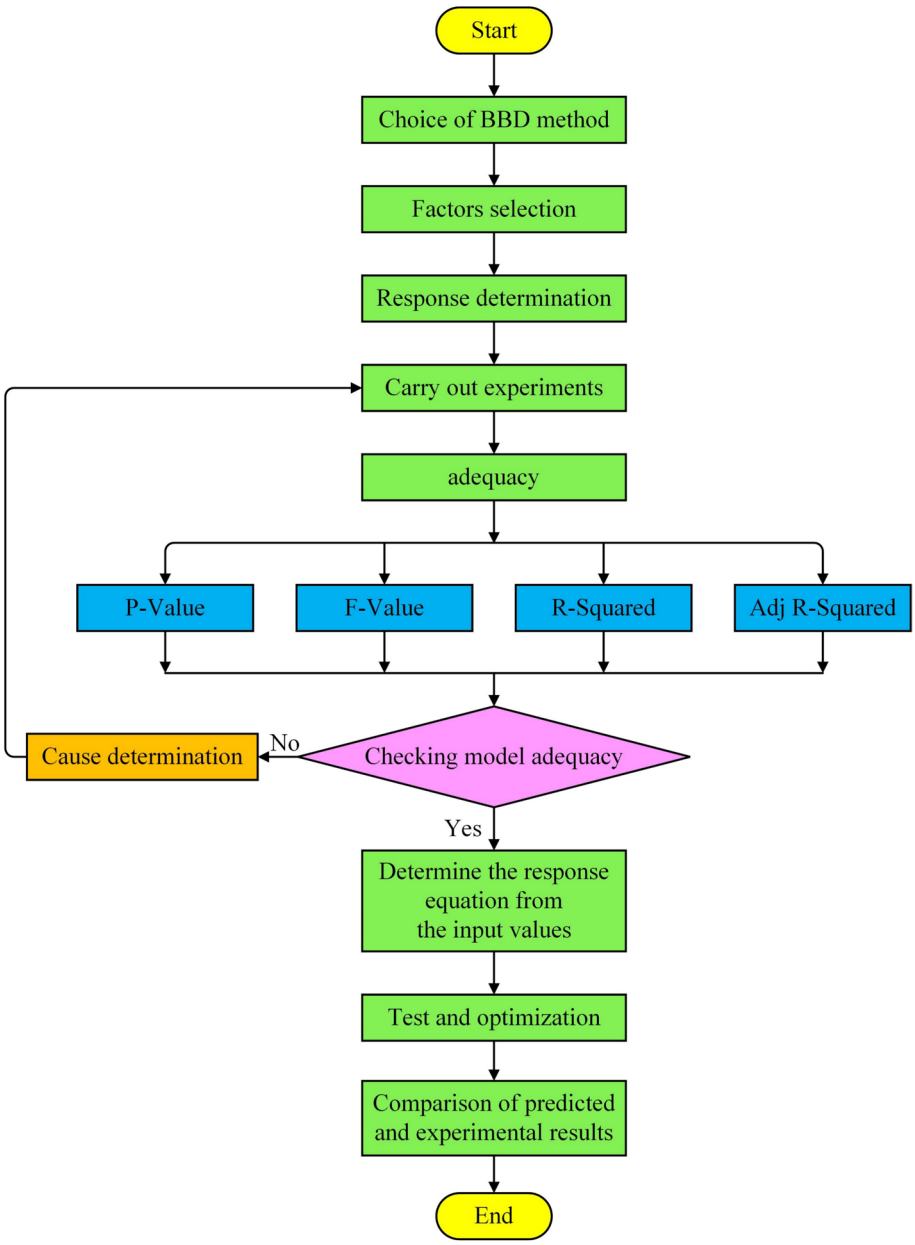

Fig. 4 Research stages flowchart

controlled at 1.2–1.4 MPa/s for compression and 0.05–0.08 MPa/s for splitting tensile strength, respectively. The test device is shown in Fig. 8.

3.4.5 Stress–Strain Curve

Prismatic specimens with dimensions of 100 mm × 100 mm × 300 mm were used to plot the mixed stress–strain diagram. Stress–strain tests were performed on specimens at 28 days of age. The tests were conducted on a YAW-1000 testing machine under displacement control at a constant rate of 0.05 mm/min. Stresses were recorded synchronously by the machine's built-in load cell and strain measurements were obtained using the digital image correlation (DIC) technique, as shown in Fig. 9.

4 Test Results

Table 6 shows the experimental design as well as the results. Thus, the results presented in the table below were the average of three samples tested.

Fig. 5 Experimental procedures

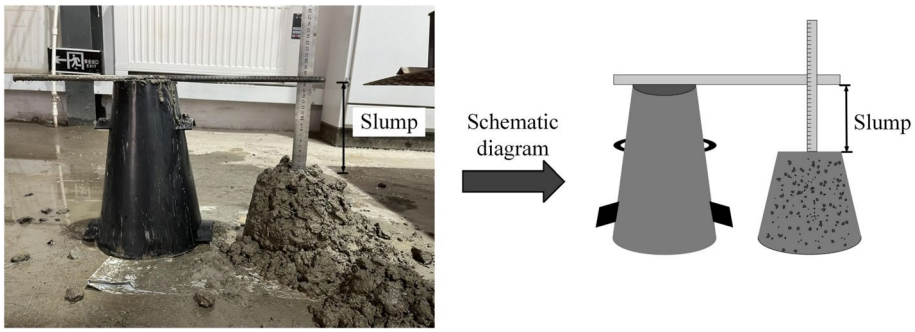

Fig. 6 Slump test

Fig. 7 Experimental device for thermal conductivity

5 Mathematical and Statistical Models Using RSM

To improve the accuracy of the test results, Table 7 presents a comprehensive multiple modeling analysis for five responses: slump (R_1), thermal conductivity (R_2), specific strength (R_3), compressive strength (R_4), and splitting tensile strength (R_5). When the p-value is less than 0.05, the regression model exhibits high statistical significance. Lower p-values indicate greater significance. For all five responses, the P-values for the quadratic model are highly significant, and the Adjusted-R^2 and Predicted-R^2 values are higher, so the quadratic polynomial model is used.

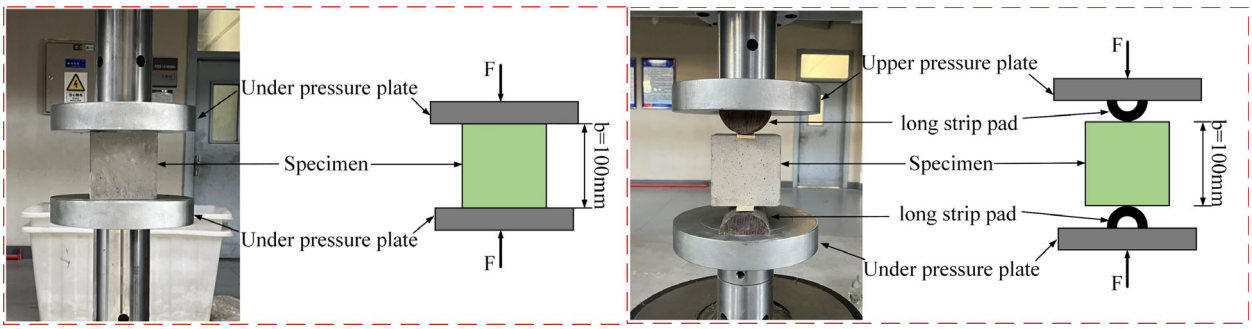

Fig. 8 Experimental diagram: **a** compressive strength test; **b** splitting tensile strength test

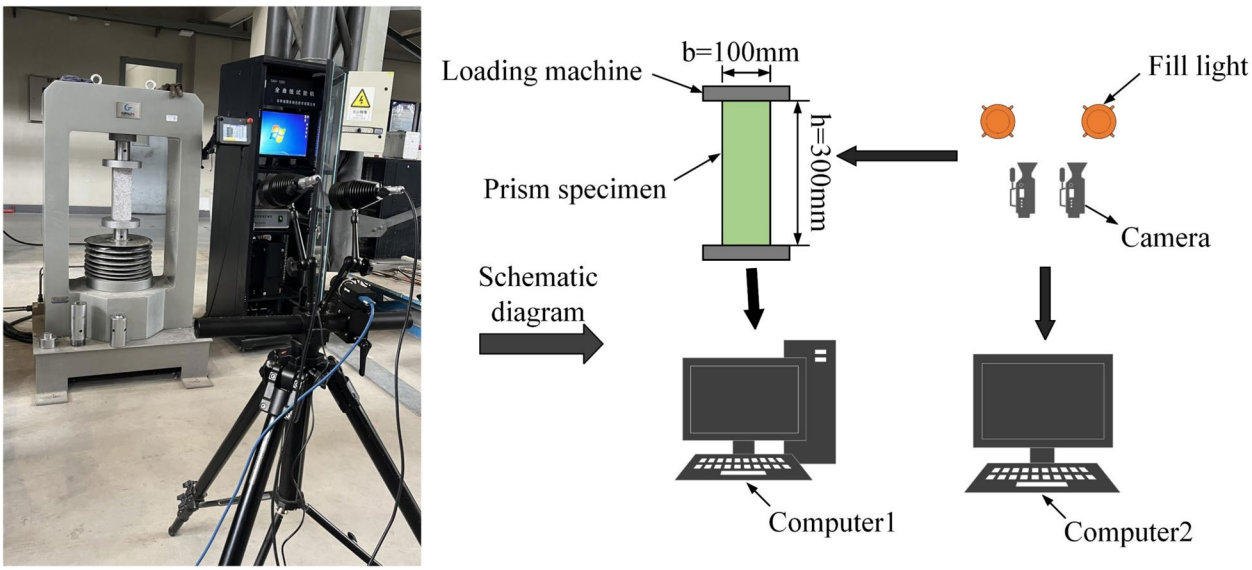

Fig. 9 Stress–strain test

5.1 Establishment, Statistical Models and Analysis of Variance

Regression fitting analysis was carried out on the experimental data, and the fitted equations for the response surfaces of slump (R_1), thermal conductivity (R_2), specific strength (R_3), compressive strength (R_4) and splitting tensile strength (R_5) were derived as shown in Table 8.

The technique employed in this part is analysis of variance (ANOVA). The ANOVA table of each experiment includes a detailed explanation of how each independent variable influences the response value. Experimental data and ANOVA analysis are modeled with a 5% error margin (Iqbal et al., 2023; Li et al., 2016). The p-value shows the importance of the tested, specified parameters in the values of the results (Balti et al., 2023). A variable is considered significant and considerably impacts the test response if its p-value is less than 5%; otherwise, the effect is less critical and not statistically significant (Libre et al., 2011).

Table 9 shows that the P values of the models for slump (R_1), thermal conductivity (R_2), specific strength (R_3), compressive strength (R_4), and splitting tensile strength (R_5) are less than 0.05. Therefore, these values are significant. Furthermore, the order of the effects on slump is B > A > C. Similarly, thermal conductivity of concrete was most significantly affected by B. It was also found that concrete specific strength, compressive strength, and splitting tensile strength of concrete were affected considerably by A.

All tests' correlation coefficients (R^2) show a connection between experimental data and anticipated behavior; the nearer this coefficient is to 1, the more precise the proposed model is (Zhang et al., 2020). The smaller the coefficient of variation and the signal-to-noise ratio is

Table 6 Measured results

No.	w/c	Rvs (%)	Vsf (%)	Slump (mm)	Thermal conductivity (W/(mK))	Specific strength (MPa/(t/m^3))	Compressive strength (MPa)	Splitting tensile strength (MPa)
1	0.35	25	1	150	0.3369	22.84	51.79	4.61
2	0.45	25	1	175	0.3111	19.71	43.67	3.74
3	0.35	75	1	124	0.2988	24.98	48.12	4.12
4	0.45	75	1	143	0.2723	21.12	39.49	3.16
5	0.35	50	0.5	156	0.3137	22.84	47.55	4.01
6	0.45	50	0.5	179	0.2879	19.46	39.49	3.18
7	0.35	50	1.5	122	0.3339	23.86	51.34	4.34
8	0.45	50	1.5	153	0.3089	20.17	42.34	3.45
9	0.4	25	0.5	180	0.3177	20.02	44.97	3.79
10	0.4	75	0.5	146	0.2805	23.38	44.36	3.52
11	0.4	25	1.5	154	0.3379	20.23	46.91	4.08
12	0.4	75	1.5	142	0.3041	23.36	46.06	3.92
13	0.4	50	1	166	0.3092	23.62	48.41	4.07
14	0.4	50	1	164	0.3087	23.57	48.28	4.13
15	0.4	50	1	165	0.3089	23.74	48.65	4.09
16	0.4	50	1	166	0.3094	23.52	48.16	4.11
17	0.4	50	1	163	0.3094	23.45	48.11	4.16

Table 7 Comprehensive analysis of multiple models of response

Response	Source	P-value	Lack of fit	Adjusted-R^2	Predicted-R^2	Evaluation
Slump (R_1)	Linear	0.0001	0.0006	0.7329	0.6336	
	2FI	0.6426	0.0004	0.7041	0.4152	
	Quadratic	0.0051	0.0038	0.9248	0.4951	Suggested
	Cubic	0.0038		0.9940		Aliased
Thermal conductivity (R_2)	Linear	< 0.0001	0.0002	0.9753	0.9582	
	2FI	0.9539	< 0.0001	0.9689	0.9008	
	Quadratic	0.0001	0.0080	0.9974	0.9826	Suggested
	Cubic	0.0080		0.9997		Aliased
Specific strength (R_3)	Linear	0.0004	0.0002	0.6829	0.6061	
	2FI	0.9870	< 0.0001	0.5931	0.2978	
	Quadratic	0.0010	0.0021	0.9360	0.5653	Suggested
	Cubic	0.0021		0.9962		Aliased
Compressive strength (R_4)	Linear	< 0.0001	0.0003	0.7846	0.7287	
	2FI	0.9931	0.0002	0.7224	0.5034	
	Quadratic	0.0057	0.0016	0.9274	0.5050	Suggested
	Cubic	0.0016		0.9963		Aliased
Splitting tensile strength (R_5)	Linear	< 0.0001	0.0017	0.7983	0.7380	
	2FI	0.9845	0.0009	0.7416	0.5075	
	Quadratic	0.0027	0.0126	0.9458	0.6488	Suggested
	Cubic	0.0126		0.9921		Aliased

greater than or equal to 4, the better the fit of the regression equation and the higher the reliability and precision of the test (Wang et al., 2020). So, it can be concluded from Table 10 that the constructed models have high accuracy and reliability. The "Normal versus Residual plot" and the "Actual versus Predicted plot", shown in Fig. 10, are two effective model diagnostic tools used to evaluate further the effectiveness and quality of the

Table 8 Each response regression equation

Regression equation
$R_1 = 164.8 + 12.25A - 13B - 11.25C - 1.5AB + 2AC + 5.5BC - 9.9A^2 - 6.9B^2 - 2.4C^2$
$R_2 = 0.3091 - 0.0129A - 0.0185B + 0.0106C - 0.0002AB + 0.0002AC + 0.0008BC - 0.0016A^2 - 0.0027B^2 + 0.0036C^2$
$R_3 = 23.58 - 1.76A + 1.26B + 0.24C - 0.1825AB - 0.0775AC - 0.0575BC - 0.7912A^2 - 0.6263B^2 - 1.21C^2$
$R_4 = 48.32 - 4.23A - 1.16B + 1.29C - 0.1275AB - 0.235AC - 0.06BC - 1.47A^2 - 1.08B^2 - 1.67C^2$
$R_5 = 4.11 - 0.4437A - 0.1875B + 0.1613C - 0.0225AB - 0.015AC + 0.0275BC - 0.1435A^2 - 0.061B^2 - 0.2235C^2$

Table 9 Variance analysis of regression model

R	F-v	P-v	S	F-v	P-v	IT	F-v	P-v	ST	F-v	P-v
R_1	22.86	0.0002	A	56.10	0.0001	AB	0.4206	0.5373	A^2	19.28	0.0032
			B	63.18	< 0.0001	AC	0.7477	0.4159	B^2	9.37	0.0183
			C	47.31	0.0002	BC	5.65	0.0490	C^2	1.13	0.3224
R_2	671.23	< 0.0001	A	1585.70	< 0.0001	AB	0.1462	0.7135	A^2	13.64	0.0077
			B	3263.17	< 0.0001	AC	0.1909	0.6753	B^2	36.56	0.0005
			C	1077.81	< 0.0001	BC	3.45	0.1057	C^2	66.12	< 0.0001
R_3	26.98	0.0001	A	121.34	< 0.0001	AB	0.6542	0.4452	A^2	12.94	0.0088
			B	61.87	0.0001	AC	0.1180	0.7413	B^2	8.11	0.0248
			C	2.26	0.1762	BC	0.0649	0.8062	C^2	30.08	0.0009
R_4	23.70	0.0002	A	155.57	< 0.0001	AB	0.0708	0.7978	A^2	9.97	0.0160
			B	11.80	0.0109	AC	0.2405	0.6388	B^2	5.34	0.0540
			C	14.38	0.0068	BC	0.0157	0.9039	C^2	12.74	0.0091
R_5	31.99	< 0.0001	A	188.16	< 0.0001	AB	0.2419	0.6379	A^2	10.36	0.0147
			B	33.59	0.0007	AC	0.1075	0.7526	B^2	1.87	0.2136
			C	24.85	0.0016	BC	0.3613	0.5667	C^2	25.12	0.0015

R response; *F-v* F-value, *P–v* P-value, *S* = Single factor, *IT* Interaction term, *ST* square term

Table 10 Reliability test and analysis of the model

Response	Std. Dev.	Mean	R^2	Adjusted-R^2	C.V. %	Adeq precision
R_1	4.63	155.75	0.9671	0.9248	2.97	17.1928
R_2	0.0009	0.3088	0.9988	0.9974	0.2964	92.7083
R_3	0.4513	22.35	0.9720	0.9360	2.02	17.4079
R_4	0.9584	46.34	0.9682	0.9274	2.07	15.1370
R_5	0.0915	3.91	0.9763	0.9458	2.34	19.3974

produced response models (Rahim et al., 2022). The linearity of the data points along the fit line demonstrates all graphs' quality of the constructed models. The regression model can accurately predict the response values because there is no statistically significant difference between the size of the projected and actual values. The data points on

(See figure on next page.)

Fig. 10 Normal plot distributions: **a** "Normal versus Residual plot" for workability; **b** "Actual versus Predicted plot" for workability; **c** "Normal versus Residual plot" for thermal conductivity; **d** "Actual versus Predicted plot" for thermal conductivity; **e** "Normal versus Residual plot" for specific strength; **f** "Actual versus Predicted plot" for specific strength; **g** "Normal versus Residual plot" for compressive strength; **h** "Actual versus Predicted plot" for compressive strength; **i** "Normal versus Residual plot" for splitting tensile strength and **j** "Actual versus Predicted plot" for splitting tensile strength

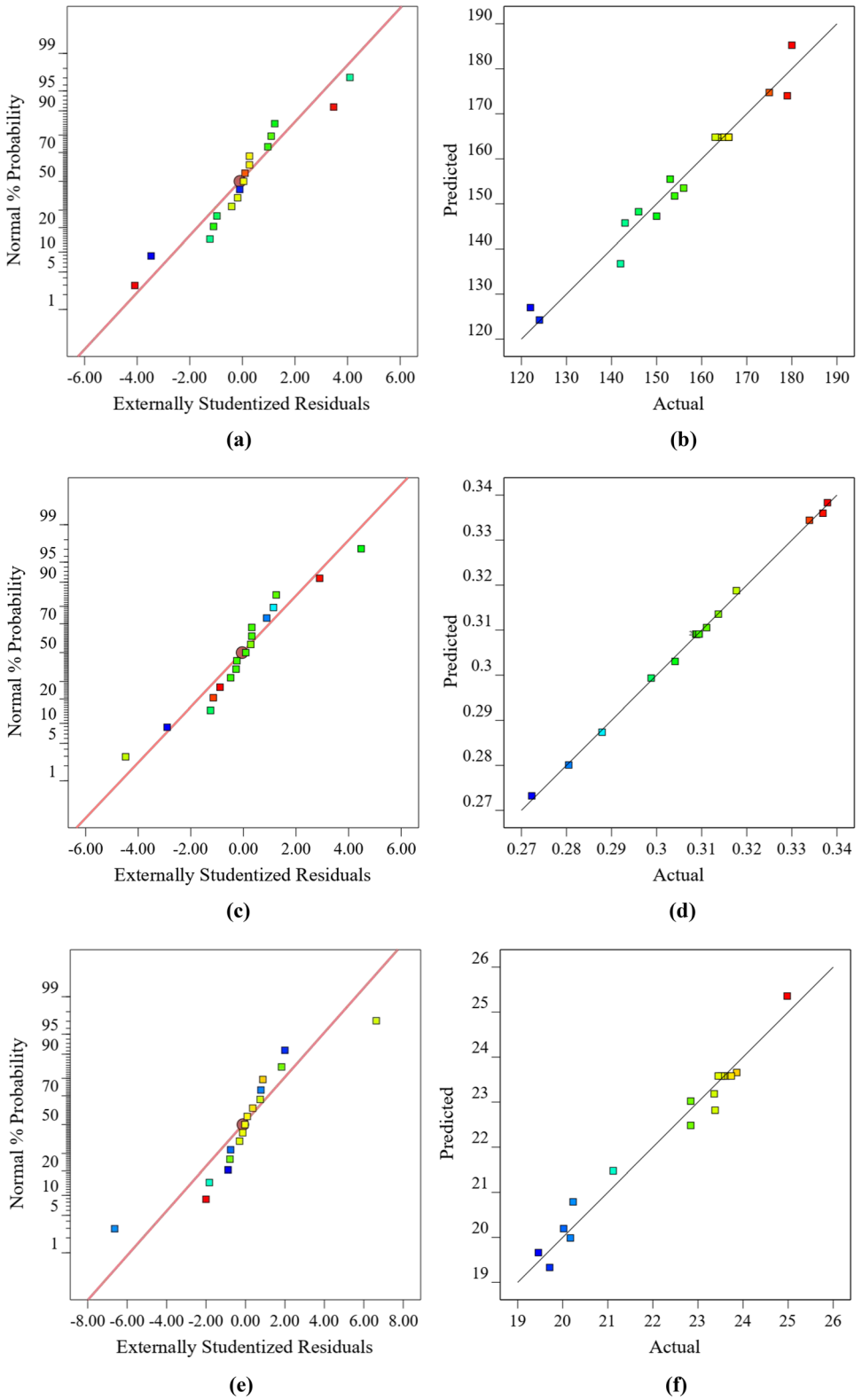

Fig. 10 (See legend on previous page.)

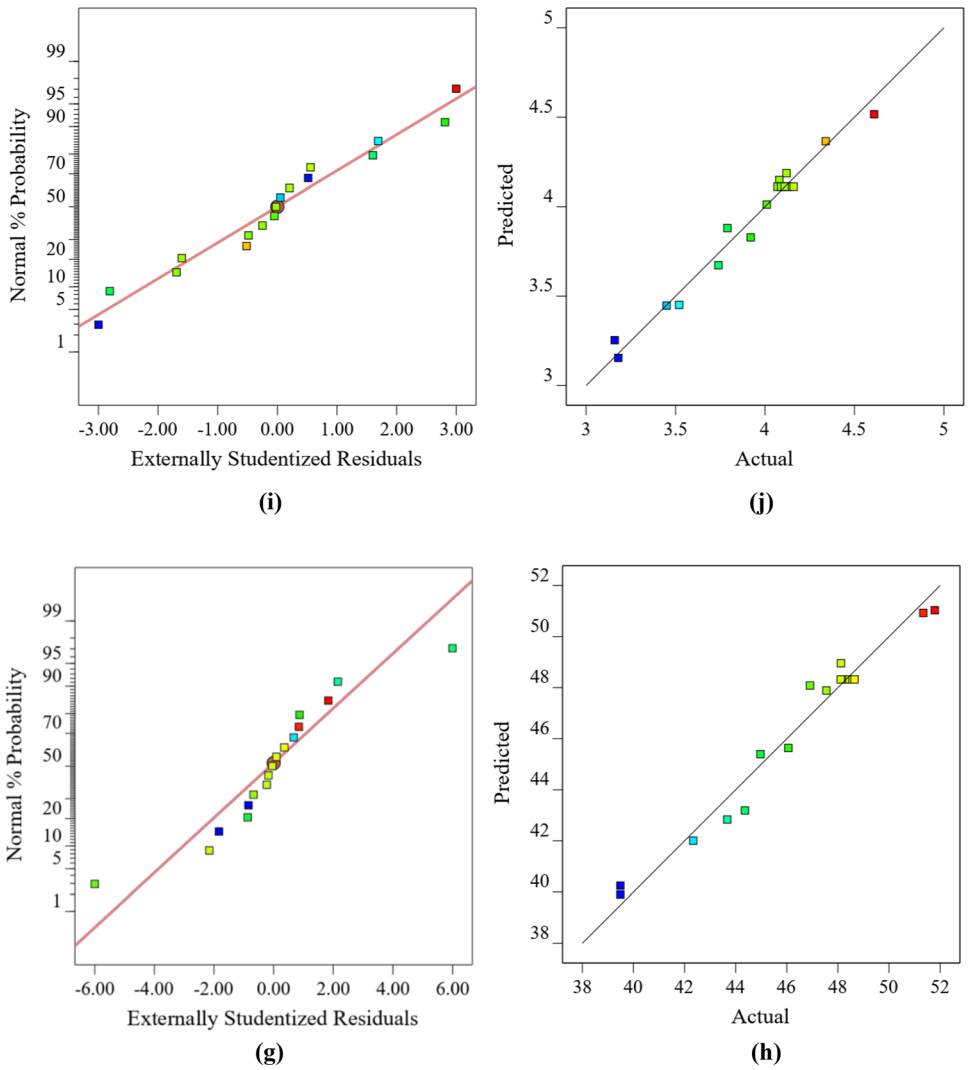

Fig. 10 continued

the standard plots of residuals that 95% of the points lie between −2 and +2 indicate that the error terms are normally distributed, which is desirable (Abdulkadir et al., 2021).

5.2 Response Surface Analysis

The RSM approach displays the impact of two input factors on the answer using 2D contour diagrams (CD) and 3D response surface plots (RSP) (Li et al., 2016; Rahim et al., 2022). The response surface diagram can show intuitively how much a component impacts the response value—the surface slope increases in proportion to the importance of the influencing element. The contour line's shape can determine the strength of the interaction between the two factors (Shahrul et al., 2021).

5.2.1 Workability of Concrete

Figure 11a shows that slump increases as the w/c increases. The reason is that the unit consumption of water in the test always remains constant; after the w/c increases, the amount of cementitious material decreases, and free water is adsorbed during concrete mixing; because of the excess free water in the concrete at this time, a large number of voids are formed within the concrete, so the lubrication between aggregates increases, friction decreases, and slump increases. Similar results were reported by Rmili et al. (2009) and Bédérina et al. (2005). Increasing the Rvs results in a slump reduction. As the Rvs increases, the fineness of the mixed fine aggregate decreases. NS has been replaced by sand with a higher fineness modulus compared to NS (Warati et al., 2019). The surface of VS is coarse and more angular, and the water absorption is greater than that of NS, which is

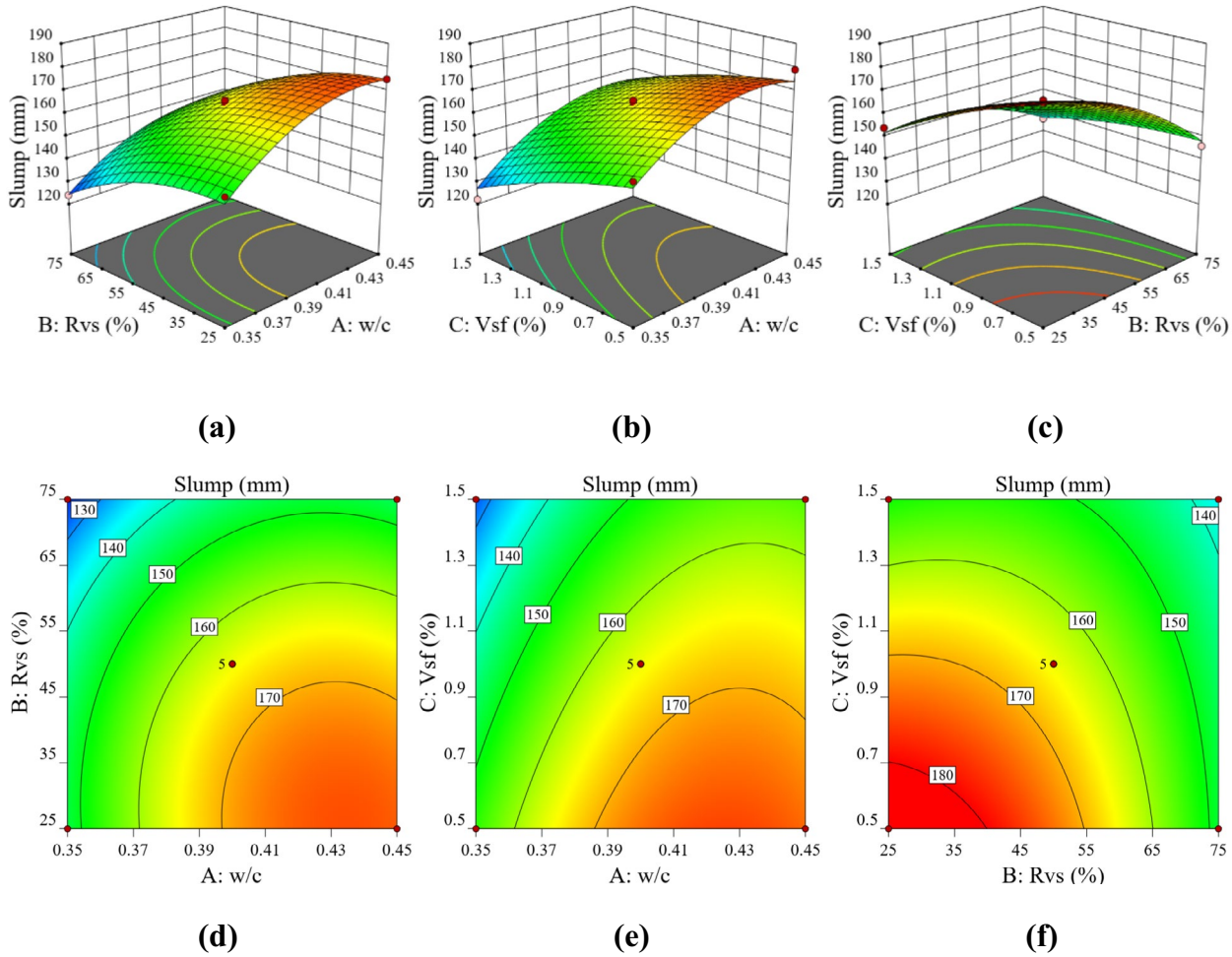

Fig. 11 RSP and CD of slump: **a** RSP of interaction between w/c and Rvs; **b** RSP of interaction between w/c and Vsf; **c** RSP of interaction between Rvs and Vsf; **d** CD of interaction between w/c and Rvs; **e** CD of interaction between w/c and Vsf and **f** CD of interaction between Rvs and Vsf

not conducive to improving the workability of concrete. This is consistent with the findings of Yifru et al. (2020) and Razavi et al. (2018). In addition, Fig. 11(b) shows that adding SF reduces slump, and it is well known that the use of SF affects the workability and flowability of concrete (Yew et al., 2011; Sagar et al., 2021). This is due to the synergistic effect of SF and the concrete matrix, which increases the bond strength at the interface transition zone and improves the strength of the concrete.

5.2.2 Thermal Conductivity

Figure 12 (a) reflects that increasing the w/c decreases the thermal conductivity. The higher the w/c, the more water must evaporate after the end of the hydration of the cement. The more holes and pores remain in the cement matrix after water evaporation, the higher the material's porosity. At the same time, the thermal conductivity of the gas is much lower than that of a solid at all temperatures, leading to a lower coefficient of thermal conductivity. Xiao et al. (2010) and Cao et al. (2022) reported similar results. Fig. 12 (b) shows that the thermal conductivity decreases as Rvs increases. This is because VS has low density and is a porous material; as the Rvs increases, it produces high material porosity and low densification, so the dry apparent density is small. With the decrease in apparent density, the thermal conductivity will decrease (Chin et al., 2020; Wang et al., 2020), and the thermal insulation performance will be better. The inclusion of SF increases the thermal conductivity because the heat passes mainly through the interior of the SF, i.e., SF provides a short path for heat flow, known as a thermal bridging effect, indicating that the addition of SF can significantly increase the thermal conductivity of the material, thus

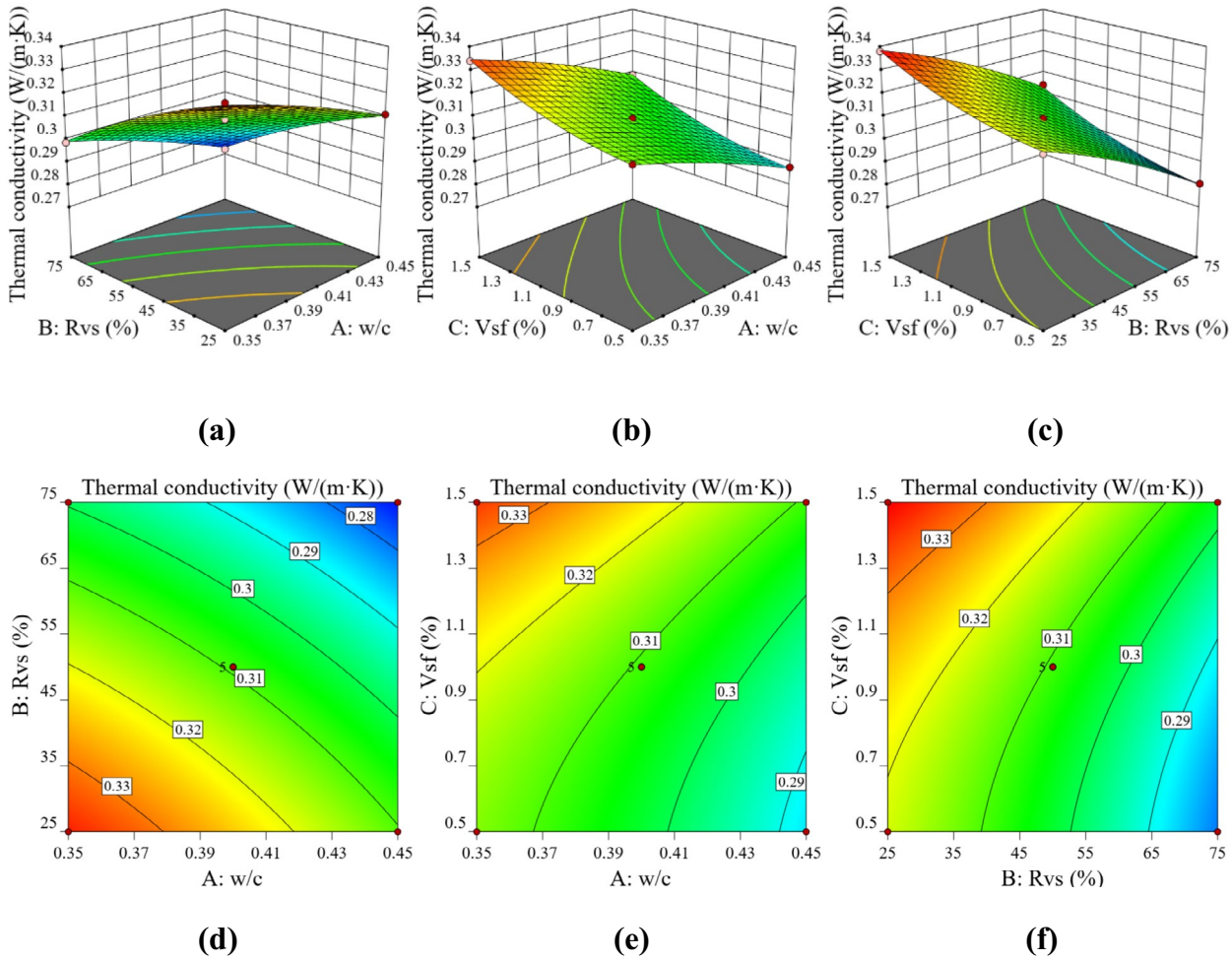

Fig. 12 RSP and CD of thermal conductivity: **a** RSP of interaction between w/c and Rvs; **b** RSP of interaction between w/c and Vsf; **c** RSP of interaction between Rvs and Vsf; **d** CD of interaction between w/c and Rvs; **e** CD of interaction between w/c and Vsf and **f** CD of interaction between Rvs and Vsf

decreasing the thermal insulation performance. This is consistent with the findings of Zhu et al. (2020).

5.2.3 Specific Strength

Increasing the specific strength of concrete helps to reduce the deadweight of concrete when determining the design life of concrete elements. It reduces the cross-sectional area of concrete supporting the elements, resulting in a relative saving of concrete volume (Warati et al., 2019). Specific strength is one of the important parameters characterizing the mechanical strength and performance of lightweight concrete materials. Fig. 13(a) shows an increased w/c reduces the specific strength. The w/c is the dominant factor affecting strength, and an increase in the w/c decreases the dry density of the specimen (Wang et al., 2022). Still, the strength of the specimen reduces more significantly, resulting in a decreasing trend in the specific strength consistent with the strength of the specimen block. The specific strength gradually increases with an increase in Rvs. This is mainly because VS has a porous structure and low strength in itself, which leads to a decrease in the strength of concrete. However, the density of VS is low, the specific gravity is low, and with increasing Rvs, the mass of concrete decreases significantly, and the lower the mass of the specimen, the lower its dry apparent density. This finding confirms the study of Shannag et al. (2014). The reduction in the strength of the specimen is less than the decrease in the dry density, so the specific strength of concrete continues to increase with the addition of VS. Warati et al. (2019) reported such results. Figure 13(b) shows that SF has increased the specific strength of the concrete. This is mainly due to increased concrete compressive strength

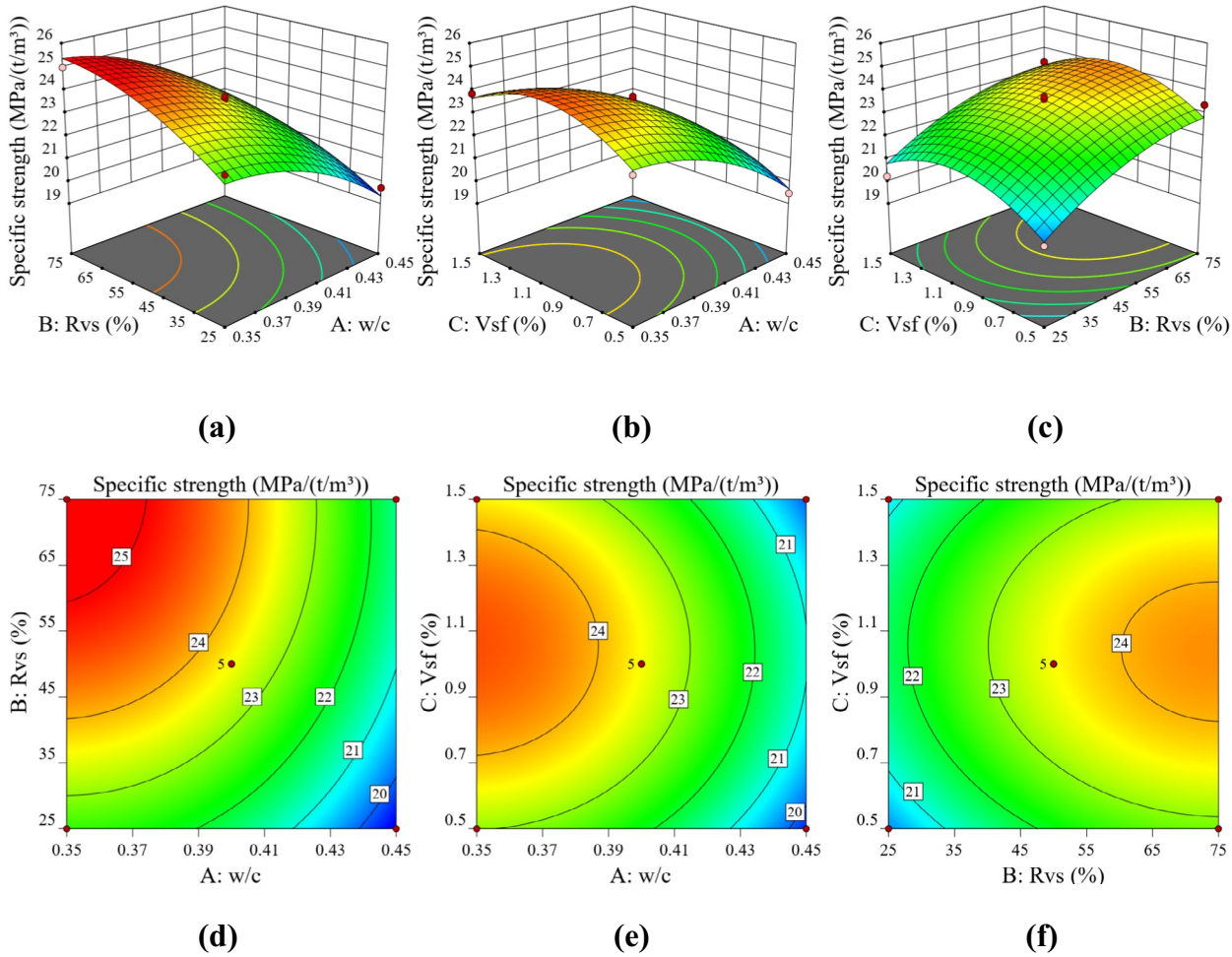

Fig. 13 RSP and CD of specific strength: **a** RSP of interaction between w/c and Rvs; **b** RSP of interaction between w/c and Vsf; **c** RSP of interaction between Rvs and Vsf; **d** CD of interaction between w/c and Rvs; **e** CD of interaction between w/c and Vsf and **f** CD of interaction between Rvs and Vsf

after adding SF. After the addition of SF, their three-dimensional chaotic distribution formed the skeleton of the fiber network, which reduced the formation and development of microcracks, prevented the formation of internal defects, and improved concrete mechanics.

5.2.4 Compressive Strength

Figure 14(a) shows that compressive strength decreases as the w/c increases. As the water-cement ratio increases, the cementitious material decreases after hydration, and the bond between the matrix reduces, resulting in a decrease in strength. Moreover, the internal porosity of high w/c concrete increases, the water retention capacity becomes poor, concrete increases, the water retention capacity becomes poor, the early water is easily dispersed, and the hydration reaction is not sufficient. Mohammed et al. (2012) and Bektas et al. (2014) also reported such results. In addition, compressive strength tends to decrease with the increase of Rvs, but with a slower trend, is because VS is added as a fine aggregate; increasing the proportion of VS increases the internal voids of concrete, and compaction deteriorates, reducing the strength of concrete. Similar to the view reported by Razavi et al. (2018). As shown in Fig. 14(b), the addition of SF leads to an increase in compressive strength. SF is distributed haphazardly throughout the concrete to improve the integrity of the matrix and vastly reduce the formation and development of cracks, enhancing the strength of the concrete. However, when the percentage of SF increases to more than 1%, the change of compressive strength tends to flatten out, which indicates that the role of SF in increasing strength gradually weakens as the amount of admixture increases. Results have shown that adding SF above a certain limit has a negative effect

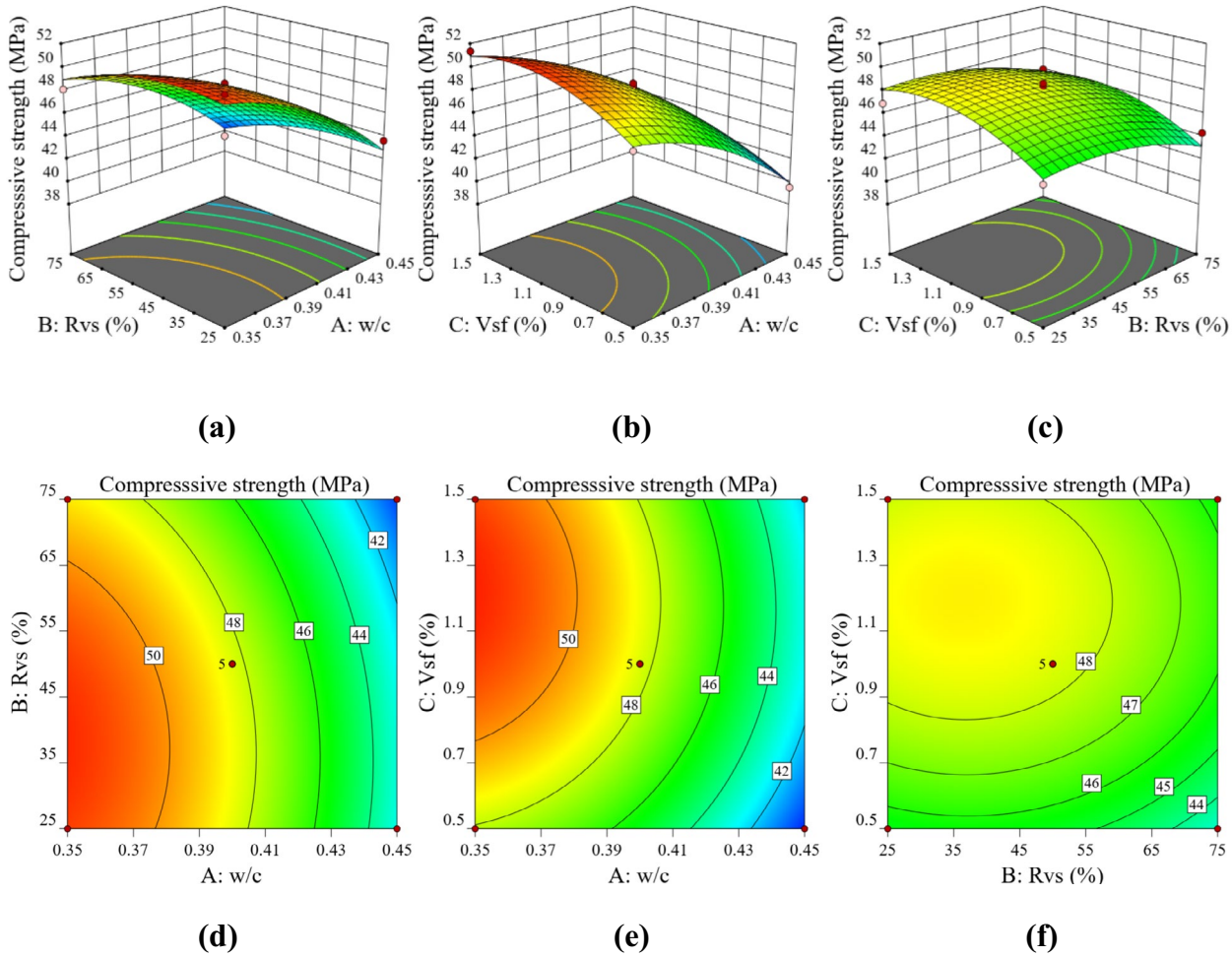

Fig. 14 RSP and CD of compressive strength: **a** RSP of interaction between w/c and Rvs; **b** RSP of interaction between w/c and Vsf; **c** RSP of interaction between Rvs and Vsf; **d** CD of interaction between w/c and Rvs; **e** CD of interaction between w/c and Vsf and **f** CD of interaction between Rvs and Vsf

on compressive strength (Noushini et al., 2013; Li et al., 1992). Adding a higher Vsf can lead to poor dispersion of the SF, which can become defective (Atahan et al., 2013), increasing the risk of pore concentration in the matrix (Noushini et al., 2013) and the formation of weaker interfacial bonding between the SF and the matrix, leading to a decrease in the compressive strength of the material under compressive loading. This is consistent with the results of Liu et al. (2019).

5.2.5 Splitting Tensile Strength

The change in splitting tensile strength of SFVSSC is similar in trend to the change in compressive strength. Figure 15(a) shows that the splitting tensile strength decreases with increasing w/c. The increase in the w/c leads to faster water evaporation. Among the factors affecting the early plastic shrinkage of concrete, the rate of water evaporation is a direct influence. Reducing the w/c makes early water evaporation more difficult, and the internal structure becomes more compact, which can reduce early plastic shrinkage, improve splitting tensile strength, and enhance resistance to internal shrinkage and deformation resistance. Increasing the Rvs also reduces splitting tensile strength. Further increases in the Rvs lead to a decrease in the work performance of the concrete mix, an increase in porosity within the concrete, and a reduction in splitting tensile strength. Razavi et al. (2018) also reported such results. Figure 15(b) shows that the splitting tensile strength increases rapidly when Vsf is increased from 0 to 1%, which is attributed to the introduction of SF to increase the toughness of the concrete. However, when the Vsf increases above 1%, the increase in splitting tensile strength of the concrete tends to level off and has a decreasing trend. Adding more steel fibers

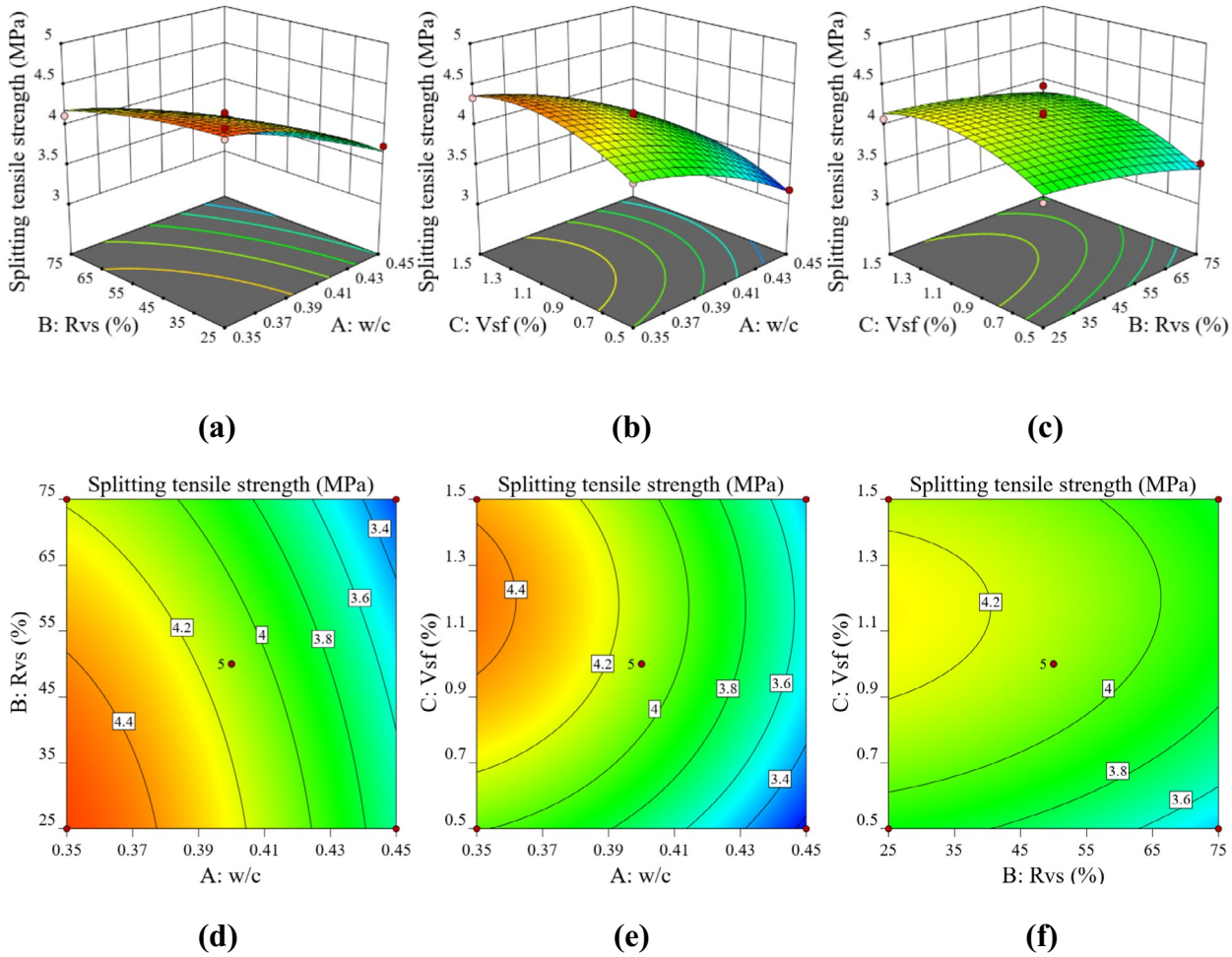

Fig. 15 RSP and CD of splitting tensile strength: **a** RSP of interaction between w/c and Rvs; **b** RSP of interaction between w/c and Vsf; **c** RSP of interaction between Rvs and Vsf; **d** CD of interaction between w/c and Rvs; **e** CD of interaction between w/c and Vsf and **f** CD of interaction between Rvs and Vsf

results in a balling effect, resulting in poor concrete compaction, internal voids, and the formation of fiber-matrix interphase. As a result, the higher the steel fiber content, the lower the splitting tensile strength of the concrete (Zhang et al., 2018; Atahan et al., 2013). This is consistent with the results of Liu et al. (2019).

5.2.6 Stress–Strain Curve

Compressive stress–strain tests were conducted to obtain compressive stress–strain curves. Figure 16 shows the stress–strain curves for different mixtures under uniform compressive loading. The stress–strain curve for each mixture represents the average of three specimens. The curves exhibit three distinct phases: the linear elastic phase, the pre-peak elastoplastic crack propagation phase, and the post-peak softening phase. As shown, increasing the the Rvs increases from 25 to 75% reduces the slope of the ascending segment, indicating a decrease in concrete elastic modulus. Although peak stress decreases significantly, peak strain increases, shifting the curve to the right. This phenomenon indicates that, compared to NS, the porous nature of VS particles permits greater deformation before failure, thereby enhancing the matrix's deformation capacity. This aligns with the findings of Tao et al. (2022). Unlike aggregate replacement, the addition of SF has a negligible effect on the pre-peak rise phase, as this phase is primarily governed by the matrix strength. However, the influence of SF becomes highly significant in the post-peak softening phase. As the Vsf increases, the peak strain slightly increases and the peak point shifts to the right. The most pronounced improvement occurs in the decline phase. Specimens containing 0.5% SF exhibit a faster stress decline, while those with 1.5% SF show a gentler slope and maintain

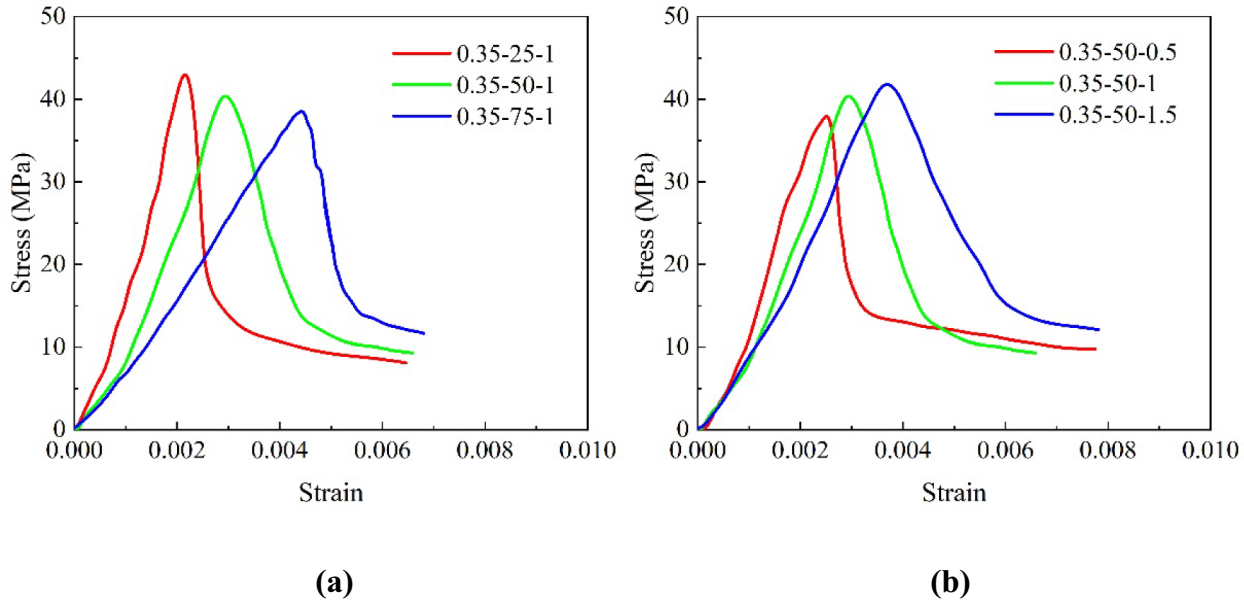

Fig. 16 Stress–strain curves: **a** different Rvs and **b** different Vsf

Table 11 Optimal design results of response surface design

w/c	Rvs (%)	Vsf (%)	Slump (mm)	Thermal conductivity (W/(mK))	Specific strength (MPa/(t/m^3))	Compressive strength (MPa)	Splitting tensile strength (MPa)	Desirability
0.35	52.8	1.15	137	0.332	24.686	51.246	4.426	0.925

higher residual stress under large deformations. This indicates that higher Vsf significantly enhances ductility and energy absorption capacity. This behavior is attributed to the bridging effect of SF. When the matrix cracks, SF bridge microcracks, effectively transferring stress and preventing brittle failure. This transforms the failure mode from brittle to quasi-ductile, consistent with reports by Basser et al. (2022).

6 Multi-Objective Optimization and Verification

Multi-objective optimization of mix proportions of SFVSSC based on regression model combined with craving function to simultaneously obtain optimal values from regression model for slump (R_1), thermal conductivity (R_2), specific strength (R_3), compressive strength (R_4) and splitting tensile strength (R_5) of SFVSSC for the optimization of the w/c, the Rvs and the Vsf (Yifru et al., 2020; Chen et al., 2022). The optimum proportioning scheme was determined: w/c of 0.35, Rvs of 52.8%, and Vsf of 1.15%. As a result, SFVSSC was prepared using the optimized parameters of the proportioning scheme, and its properties were measured; the results are shown in Table 11.

Table 12 Test verification of optimal design results

Response value	V_P	V_E	E (%)
Slump (mm)	137	143	4.12
Thermal conductivity (W/(m·K))	0.332	0.324	2.47
Specific strength (MPa/(t/m^3))	24.686	25.852	4.51
Compressive strength (MPa)	51.246	53.19	3.65
Splitting tensile strength (MPa)	4.426	4.22	4.88

To further verify the accuracy of the model, an experimental verification of the mix proportion given in Table 11 was carried out according to Eq. 5, and the experimental values were compared with the predicted values, with the results shown in Table 12 and Fig. 17, using the absolute value of the relative error:

$$E = \frac{|V_E - V_P|}{V_E} \times 100\% \tag{5}$$

where E is the absolute value of relative error, V_E is the experimental value, V_P is the predicted value.

As seen from Table 12, after the optimal set of experimental validation, the absolute value of the relative error

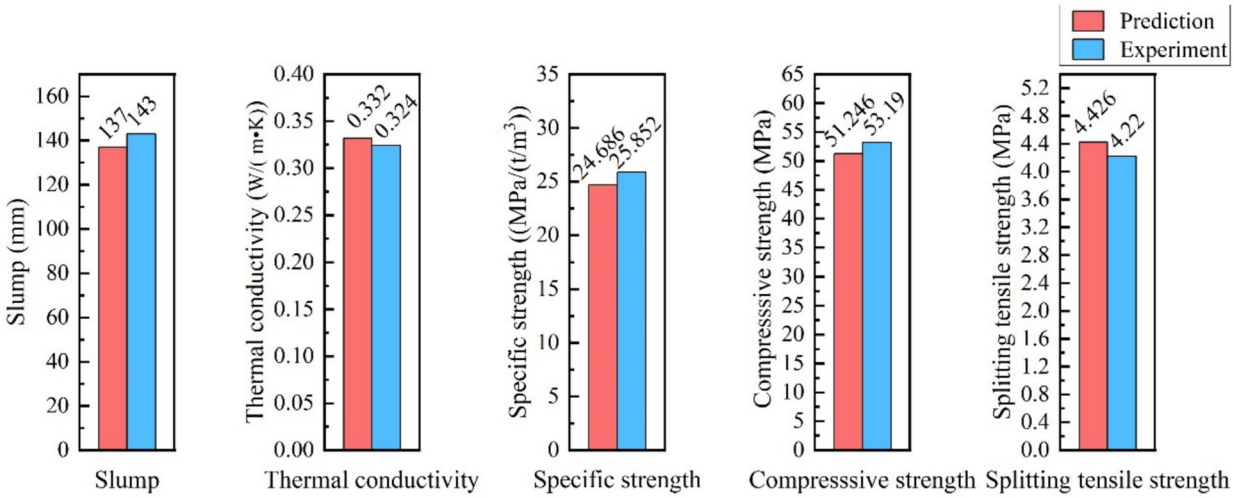

Fig. 17 RSM predicted values and experimental results for the optimized mixture

between the experimental values and the predicted values is less than 5%, indicating that the regression model's prediction accuracy is high. The optimal dosage for RSM multi-objective optimization, as well as the predicted response values, are reliable. Therefore, multi-objective optimization of response surface methodology can obtain SFVSSC with preferred multi-objective.

7 Conclusions

This paper studies the mix proportion of SFVSSC. The variables studied are the w/c, the Rvs, and the Vsf at three different levels. The most important conclusions drawn from this study are as follows.

1. The BBD model established in this study demonstrates high predictive accuracy for SFVSSC performance. The R^2 values for slump, thermal conductivity, specific strength, compressive strength, and splitting tensile strength were 0.9671, 0.9988, 0.9720, 0.9682, and 0.9763, respectively, confirming the reliability of the developed model.
2. The incorporation of VS significantly influences physical and mechanical properties, enabling its use as a partial replacement for NS in concrete mixes. Increasing Rvs effectively reduces thermal conductivity, thereby enhancing insulation performance. However, this also leads to decreases in slump and mechanical strength. Notably, due to lightweight nature of VS, increasing Rvs improves specific strength, providing a balance between reducing self-weight and maintaining structural performance.
3. Adding SF can improve the performance of volcanic scoria sand concrete. As the Vsf increased, the compressive and splitting tensile strength of SFVSSC increased essentially linearly. Besides, the increase slowed when SF was added in amounts greater than 1%. The incorporation of SF resulted in a significant increase in the mechanical properties of the concrete, while the thermal conductivity increased, resulting in a decrease in the thermal insulation properties of the material. Slight inhibition of the slump was observed. From the point of view of the optimal use of SF, it is desirable to add about 1%.
4. Multi-objective optimization was performed using the RSM method to obtain the optimal values of the slump, thermal conductivity, specific strength, compressive strength, and splitting tensile strength. The optimum concrete proportion to satisfy the workability and mechanical properties was derived as w/c of 0.35, Rvs of 52.8%, and Vsf of 1.15%.
5. Through experimental verification of the optimal mix design, the response values predicted by the RSM under the best mix ratio showed minimal deviation from actual values and remained within a reasonable range, validating the effectiveness of the optimization approach.
6. SFVSSC demonstrates outstanding potential as an eco-friendly building material. It serves as a green construction material that meets building energy efficiency requirements (low thermal conductivity) while reducing structural weight (light self-weight with sufficient strength), offering favorable conditions and advantages for practical engineering applications.

Acknowledgements
This research was financially supported by Jilin Provincial Science and Technology Development Plan Project, award number 20250203145SF. The authors

wish to acknowledge the sponsors. However, any opinions, findings, conclusions and recommendations presented in this paper are those of the authors and do not necessarily reflect the views of the sponsors.

Author Contributions
BC and FF designed the research methodology; LX performed the analysis, LX and LW draft the manuscript; BC and FF reviewed the manuscript. All authors read and approved the final manuscript.

Funding
Founder: Jilin Provincial Science and Technology Development Plan Project, Award Number 20250203145SF.

Availability of Data and Materials
Some or all data, models, or codes that support the findings of this study are available from the authors upon reasonable request.

Declarations

Competing Interest
The authors declare that they have no known competing financial interests or personal relationships.

Received: 22 March 2024 Accepted: 15 March 2026
Published online: 27 April 2026

References

Abdulkadir, I., Mohammed, B. S., Ali, M. O. A., & Liew, M. S. (2022). Effects of graphene oxide and crumb rubber on the fresh properties of self-compacting engineered cementitious composite using response surface methodology. *Materials*. https://doi.org/10.3390/ma15072519

Abdulkadir, I., Mohammed, B. S., Liew, M., & Wahab, M. (2021). Modelling and multi-objective optimization of the fresh and mechanical properties of self-compacting high volume fly ash ECC (HVFA-ECC) using response surface methodology (RSM). *Case Studies in Construction Materials*. https://doi.org/10.1016/j.cscm.2021.e00525

Adamu, M., Mohammed, B. S., & Liew, M. S. (2018). Mechanical properties and performance of high volume fly ash roller compacted concrete containing crumb rubber and nano silica. *Construction and Building Materials, 171*, 521–538.

Adamu, M., Trabanpruek, P., & Jongvivatsakul, P. (2021). Mechanical performance and optimization of high-volume fly ash concrete containing plastic wastes and graphene nanoplatelets using response surface methodology. *Construction and Building Materials, 308*, Article 125085.

Afroughsabet, V., & Ozbakkaloglu, T. (2015). Mechanical and durability properties of high-strength concrete containing steel and polypropylene fibers. *Construction and Building Materials, 94*, 73–82.

Amiri, H., Azadi, S., Karimaei, M., Sadeghi, H., & Farshad, D. (2022). Multi-objective optimization of coal waste recycling in concrete using response surface methodology. *Journal of Building Engineering*, *45*.

Anwar Hossain, K. M. (2004). Properties of volcanic pumice based cement and lightweight concrete. *Cement and Concrete Research, 34*(2), 283–291.

Asadzadeh, S., & Khoshbayan, S. (2018). Multi-objective optimization of influential factors on production process of foamed concrete using Box-Behnken approach. *Construction and Building Materials, 170*, 101–110.

Atahan, H. N., Pekmezci, B. Y., & Tuncel, E. Y. (2013). Behavior of PVA fiber-reinforced cementitious composites under static and impact flexural effects. *Journal of Materials in Civil Engineering, 25*(10), 1438–1445.

Balti, S., Boudenne, A., & Hamdi, N. (2023). Characterization and optimization of eco-friendly gypsum materials using response surface methodology. *Journal of Building Engineering*. https://doi.org/10.1016/j.jobe.2023.106219

Basser, H., Shaghaghi, T. M., Afshin, H., Ahari, R. S., & Mirrezaei, S. S. (2022). An experimental investigation and response surface methodology-based modeling for predicting and optimizing the rheological and mechanical properties of self-compacting concrete containing steel fiber and PET. *Construction and Building Materials*. https://doi.org/10.1016/j.conbuildmat.2021.125370

Bédérina, M., Khenfer, M. M., Dheilly, R. M., & Quéneudec, M. (2005). Reuse of local sand: Effect of limestone filler proportion on the rheological and mechanical properties of different sand concretes. *Cement and Concrete Research, 35*(6), 1172–1179.

Bektas, F., & Bektas, B. A. (2014). Analyzing mix parameters in ASR concrete using response surface methodology. *Construction and Building Materials, 66*, 299–305.

Cao, X. X., Dang, J. T., & Li, F. L. (2022). Effect of water-cement ratio on the compressive strength and thermal conductivity of foamed concrete. *China Concrete and Cement Products, 11*, 68–71+75.

Chen, Y., Wu, J., Zhang, Y., Fu, L., Luo, Y., Liu, Y., & Li, L. (2022). Research on hyperparameter optimization of concrete slump prediction model based on response surface method. *Materials*. https://doi.org/10.3390/ma15134721

Chin, C. O., Yang, X., Kong, S. Y., Paul, S. C., Susilawati, & Wong, L. S. (2020). Mechanical and thermal properties of lightweight concrete incorporated with activated carbon as coarse aggregate. *Journal of Building Engineering*, *31*.

GB/T 10294-2008. (2008). *Thermal insulation—Determination of steady-state thermal resistance and related properties—Guarded hot plate apparatus*. Standards Press of China.

GB/T 50081-2019. (2019). *Standard for test methods of concrete physical and mechanical properties*. China Architecture & Building Press.

GB/T50080-2016. (2016). *Standard for test method of performance on ordinary fresh concrete*. China Architecture & Building Press.

Hari, R., & Mini, K. M. (2023). Mechanical and durability properties of basalt-steel wool hybrid fibre reinforced pervious concrete—A Box Behnken approach. *Journal of Building Engineering*, *70*.

Hassanpour, M., Shafigh, P., & Mahmud, H. B. (2012). Lightweight aggregate concrete fiber reinforcement—A review. *Construction and Building Materials, 37*, 452–461.

Huang, W., Guo, Y., & Ge, P. (2022). Mixture ratio optimization of polypropylene fiber recycled brick aggregate concrete based on response surface methodology. *Journal of Central South University (Science and Technology), 53*, 2709–2718.

Huang, X., Ranade, R., Zhang, Q., Ni, W., & Li, V. C. (2013). Mechanical and thermal properties of green lightweight engineered cementitious composites. *Construction and Building Materials, 48*, 954–960.

Huang, Y., Dong, L., Qi, X., Wang, T., Li, P., & Zhong, J. (2023). Effects of mix components on mechanical properties of marine volcanic-scoria concrete under axial compression. *Case Studies in Construction Materials*. https://doi.org/10.1016/j.cscm.2023.e01837

Iqbal, H. W., Hamcumpai, K., Nuaklong, P., Jongvivatsakul, P., Likitlersuang, S., Chintanapakdee, C., & Wijeyewickrema, A. C. (2023). Effect of graphene nanoplatelets on engineering properties of fly ash-based geopolymer concrete containing crumb rubber and its optimization using response surface methodology. *Journal of Building Engineering*. https://doi.org/10.1016/j.jobe.2023.107024

JGJ/T12-2019. (2019). *Technical standard for application of lightweight aggregate concrete*. China Architecture & Building Press.

Li, J. j., Niu, J. g., Wan, C. j., Jin, B., & Yin, Y. l. (2016). Investigation on mechanical properties and microstructure of high performance polypropylene fiber reinforced lightweight aggregate concrete. *Construction and Building Materials, 118*, 27–35.

Li, J., Zhao, E., Niu, J., & Wan, C. (2021). Study on mixture design method and mechanical properties of steel fiber reinforced self-compacting lightweight aggregate concrete. *Construction and Building Materials*, *267*.

Li, C., Li, J., Ren, Q., Zheng, Q., & Jiang, Z. (2023). Durability of concrete coupled with life cycle assessment: Review and perspective. *Cement and Concrete Composites*. https://doi.org/10.1016/j.cemconcomp.2023.105041

Li, J., Huang, J., Niu, J., & Wan, C. (2019). Mesoscopic study on axial compressive damage of steel fiber reinforced lightweight aggregate concrete. *Construction and Building Materials, 196*, 14–25.

Li, V. C. (1992). A simplified micromechanical model of compressive strength of fiber-reinforced cementitious composites. *Cement and Concrete Composites, 14*(2), 131–141.

Libre, N. A., Shekarchi, M., Mahoutian, M., & Soroushian, P. (2011). Mechanical properties of hybrid fiber reinforced lightweight aggregate concrete made with natural pumice. *Construction and Building Materials, 25*(5), 2458–2464.

Liu, X., Wu, T., & Liu, Y. (2019). Stress-strain relationship for plain and fibre-reinforced lightweight aggregate concrete. *Construction and Building Materials, 225*, 256–272.
Luo, X., Xing, G., Qiao, L., Miao, P., Yu, X., & Ma, K. (2023). Multi-objective optimization of the mix proportion for dune sand concrete based on response surface methodology. *Construction and Building Materials*. https://doi.org/10.1016/j.conbuildmat.2022.129928
Maaze, M. R., & Shrivastava, S. (2023). Design optimization of a recycled concrete waste-based brick through alkali activation using Box- Behnken design methodology. *Journal of Building Engineering, 75*.
Miller, S. A., Horvath, A., & Monteiro, P. J. M. (2016). Readily implementable techniques can cut annual CO_2 emissions from the production of concrete by over 20%. *Environmental Research Letters*. https://doi.org/10.1088/1748-9326/11/7/074029
Mohammed, B. S., Fang, O. C., Anwar Hossain, K. M., & Lachemi, M. (2012). Mix proportioning of concrete containing paper mill residuals using response surface methodology. *Construction and Building Materials, 35*, 63–68.
Noushini, A., Samali, B., & Vessalas, K. (2013). Effect of polyvinyl alcohol (PVA) fibre on dynamic and material properties of fibre reinforced concrete. *Construction and Building Materials, 49*, 374–383.
Rahim, N. I., Mohammed, B. S., Abdulkadir, I., & Dahim, M. (2022). Effect of crumb rubber, fly ash, and nanosilica on the properties of self-compacting concrete using response surface methodology. *Materials*. https://doi.org/10.3390/ma15041501
Razavi, S. V., Rahimi, A., & Samsami, M. (2018). Using scoria as fine aggregate in lightweight mortar and concrete. *Soil Structure Interaction Journal, 1*(1), 53–61.
Rmili, A., Ouezdou, M. B., Added, M., & Ghorbel, E. (2009). Incorporation of crushed sands and Tunisian desert sands in the composition of self compacting concretes Part II: SCC fresh and hardened states characteristics. *International Journal of Concrete Structures and Materials, 3*(1), 11–14.
Safari, J., Mirzaei, M., & Rooholamini, H. (2018). Effect of rice husk ash and macro-synthetic fibre on the properties of self-compacting concrete. *Construction and Building Materials, 175*, 371–380.
Sagar, B., & Sivakumar, M. V. N. (2021). Compressive properties and analytical modelling for stress-strain curves of polyvinyl alcohol fiber reinforced concrete. *Construction and Building Materials, 291*, Article 123192.
Sayadi, A. A., Tapia, J. V., Neitzert, T. R., & Clifton, G. C. (2016). Effects of expanded polystyrene (EPS) particles on fire resistance, thermal conductivity and compressive strength of foamed concrete. *Construction and Building Materials, 112*, 716–724.
Shahrul, S., Mohammed, B. S., Wahab, M. M. A., & Liew, M. S. (2021). Mechanical properties of crumb rubber mortar containing nano-silica using response surface methodology. *Materials*, *14*(19).
Shannag, M., Charif, A., Naser, S., Faisal, F., & Karim, A. (2014). Structural behavior of lightweight concrete made with scoria aggregates and mineral admixtures. *Int. J. Civ. Archit. Sci. Eng, 8*, 105–109.
Siamardi, K. (2022). Optimization of fresh and hardened properties of structural light weight self-compacting concrete mix design using response surface methodology. *Construction and Building Materials*. https://doi.org/10.1016/j.conbuildmat.2021.125928
Tao, Y. (2022). *Study on mechanical properties and constitutive relationship of steel fiber scoria aggregate concrete after fire exposure*. Dissertation for the Master Degree of Engineering. JiLin Jianzhu University.
Tchamdjou, W. H. J., Cherradi, T., Abidi, M. L., & Pereira-de-Oliveira, L. A. (2017a). The use of volcanic scoria from 'Djoungo' (Cameroon) as cement replacement and fine aggregate by sand substitution in mortar for masonry. *European Journal of Environmental and Civil Engineering, 24*(1), 60–78.
Tchamdjou, W. H. J., Grigoletto, S., Michel, F., Courard, L., Abidi, M. L., & Cherradi, T. (2017b). An investigation on the use of coarse volcanic scoria as sand in Portland cement mortar. *Case Studies in Construction Materials, 7*, 191–206.
Tunc, E. T. (2019). Recycling of marble waste: A review based on strength of concrete containing marble waste. *Journal of Environmental Management, 231*, 86–97.
Wang, Y., Zheng, T., Zheng, X., Liu, Y., Darkwa, J., & Zhou, G. (2020). Thermo-mechanical and moisture absorption properties of fly ash-based lightweight geopolymer concrete reinforced by polypropylene fibers. *Construction and Building Materials*, *251*.
Wang, X., & Li, J. C. (2022). Study on physical and mechanical properties of bamboo fiber cement-based materials. *The World of Building Materials, 5*, 9–13.
Warati, G. K., Darwish, M. M., Feyessa, F. F., & Ghebrab, T. (2019). Suitability of scoria as fine aggregate and its effect on the properties of concrete. *Sustainability*. https://doi.org/10.3390/su11174647
Wu, Y., Wang, J. Y., Monteiro, P. J. M., & Zhang, M. H. (2015). Development of ultralightweight cement composites with low thermal conductivity and high specific strength for energy efficient buildings. *Construction and Building Materials, 87*, 100–112.
Xiao, J. X., Song, Z. W., & Zhang, F. (2010). An experimental study on thermal conductivity of concrete. *Journal of Building Materials, 13*(1), 17–21.
Yew, M. K., Othman, I., Yew, M. C., Yeo, S. H., & Mahmud, H. B. (2011). Strength properties of hybrid nylon-steel and polypropylene-steel fibre-reinforced high strength concrete at low volume fraction. *International Journal of Physical Sciences, 6*(33), 7584–7588.
Yifru, B. W., & Mitikie, B. B. (2020). Partial replacement of sand with marble waste and scoria for normal strength concrete production. *SN Applied Sciences*, *2*(12).
Yu, Q. L., Spiesz, P., & Brouwers, H. J. H. (2015). Ultra-lightweight concrete: Conceptual design and performance evaluation. *Cement and Concrete Composites, 61*, 18–28.
Zhang, L., & Yue, Y. (2018). Influence of waste glass powder usage on the properties of alkali-activated slag mortars based on response surface methodology. *Construction and Building Materials, 181*, 527–534.
Zhang, Q., Feng, X., Chen, X., & Lu, K. (2020). Mix design for recycled aggregate pervious concrete based on response surface methodology. *Construction and Building Materials*. https://doi.org/10.1016/j.conbuildmat.2020.119776
Zhou, Y., Liu, X., Xing, F., Cui, H., & Sui, L. (2016). Axial compressive behavior of FRP-confined lightweight aggregate concrete: An experimental study and stress-strain relation model. *Construction and Building Materials, 119*, 1–15.
Zhu, D., Han, Y., Shen, L., Yao, X. P., & Cao, M. S. (2020). Experimental study on thermal properties of steel fiber reinforced concrete after elevated temperature. *Fire Science and Technology, 11*, 1477–1481.

Publisher's Note

Bin Cai School of Civil Engineering, Jilin Jianzhu University, Changchun, China.

Li Xu School of Civil Engineering, Jilin Jianzhu University, Changchun, China.

Lin Wang School of Economics and Management, Jilin Jianzhu University, Changchun, China.

Feng Fu Department of Engineering, School of Science and Technology, City, University of London, London, UK.